Supporting Information

Collective redox-shuttling properties of nanoalloys boost water electrolysis of nitrides

Peng Zuo[1,2], Na Li[1], Jiawei Lu[1], Jiayang Zhang[1], Zhaojun Wen[3], Huihuang Fang[4], Weizhou Jiao[1,*], Ruixin Wang[1,*], Haiqiang Lin[3], Xinping Duan[3,*]

* To whom correspondence should be addressed

E-mail: xpduan@xmu.edu.cn (X. D.), zbdxwrx@nuc.edu.cn (R. W.), zbdxjwz@nuc.edu.cn (W. J.)

1. Preparation of Ni/Co-precursor/NF

Firstly, the Ni foam (NF) (2×5 cm^2) was pre-treated by ultrasonication in ethanol, deionized water and 2 M HCl for 15 min, respectively. Secondly, 6 mmol of $CoCl_2 \cdot 6H_2O$ and $NiCl_2 \cdot 6H_2O$ with different mole ratios of Ni/Co (1:2) and 6 mmol of urea were uniformly dispersed into 40 mL of purified water under ultrasonication, and then poured into a 50 mL Teflon autoclave. After a piece of the pre-treated NF was immersed in the Teflon autoclave, the autoclave was sealed and maintained at 100 °C for 10 h. After that, it was cooled down naturally to room temperature, and the sample was subsequently rinsed with distilled water, and dried at room temperature, obtaining the Ni/Co-precursor/NF.

2. Preparation of Pt/C/NF and RuO_2/NF

The self-supported 20 wt% Pt/C and RuO_2 electrodes on NF (Pt/C/NF and RuO_2/NF) were also prepared to get a further activity evaluation. Typically, commercial 20 wt% Pt/C or RuO_2 was well dispersed in a mixture of water/isopropanol/Nafion (4:1:0.1 v/v/v) and ultrasonicated for 30 min to form a well dispersed ink. Subsequently, 100 μL of the ink was slowly loaded onto the preprocessed NFs and dried under vacuum to obtain the Pt/C/NF or RuO_2/NF working electrodes with a catalyst loading capacity of 10 mg cm^{-2}.

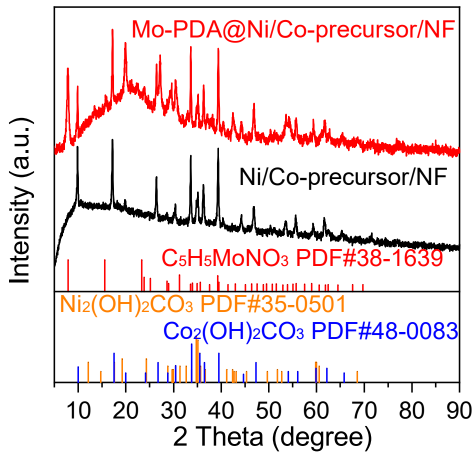

Fig. S1 XRD patterns of Ni/Co-precursor/NF.

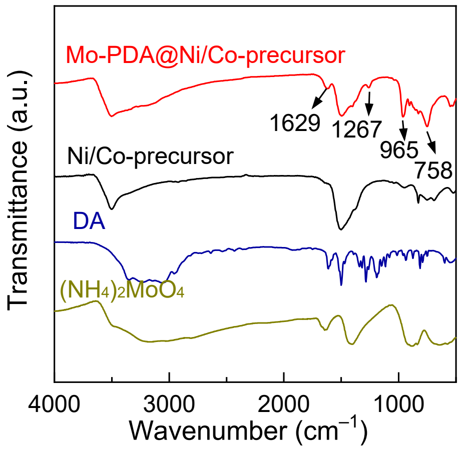

Fig. S2 FT-IR spectra of Mo-PDA@Ni/Co-precursor, Ni/Co-precursor, DA, and $(NH_2)MoO_4$.

In order to examine the FT-IR spectrum, the specimens are scraped from Ni foam. Compared to the FT-IR spectrum of Ni/Co-precursor, some new characteristic peaks appear in that of Mo-PDA@Ni/Co-precursor, for example, the peaks at 1629 and 1267 cm^{-1} corresponding to C=C and C−OH groups of DA, respectively, and the peaks at 965 and 758 cm^{-1} assigned to Mo=O and Mo−O−Mo groups of molybdenum oxide, respectively, indicating that PDA and ammonium molybdate are coated on Ni/Co-precursor. In addition, the peaks at 1629 and 1267 cm^{-1} of Mo-PDA@Ni/Co-precursor has shifted compared with that of the pure DA, due to the formation of Mo-PDA complex.

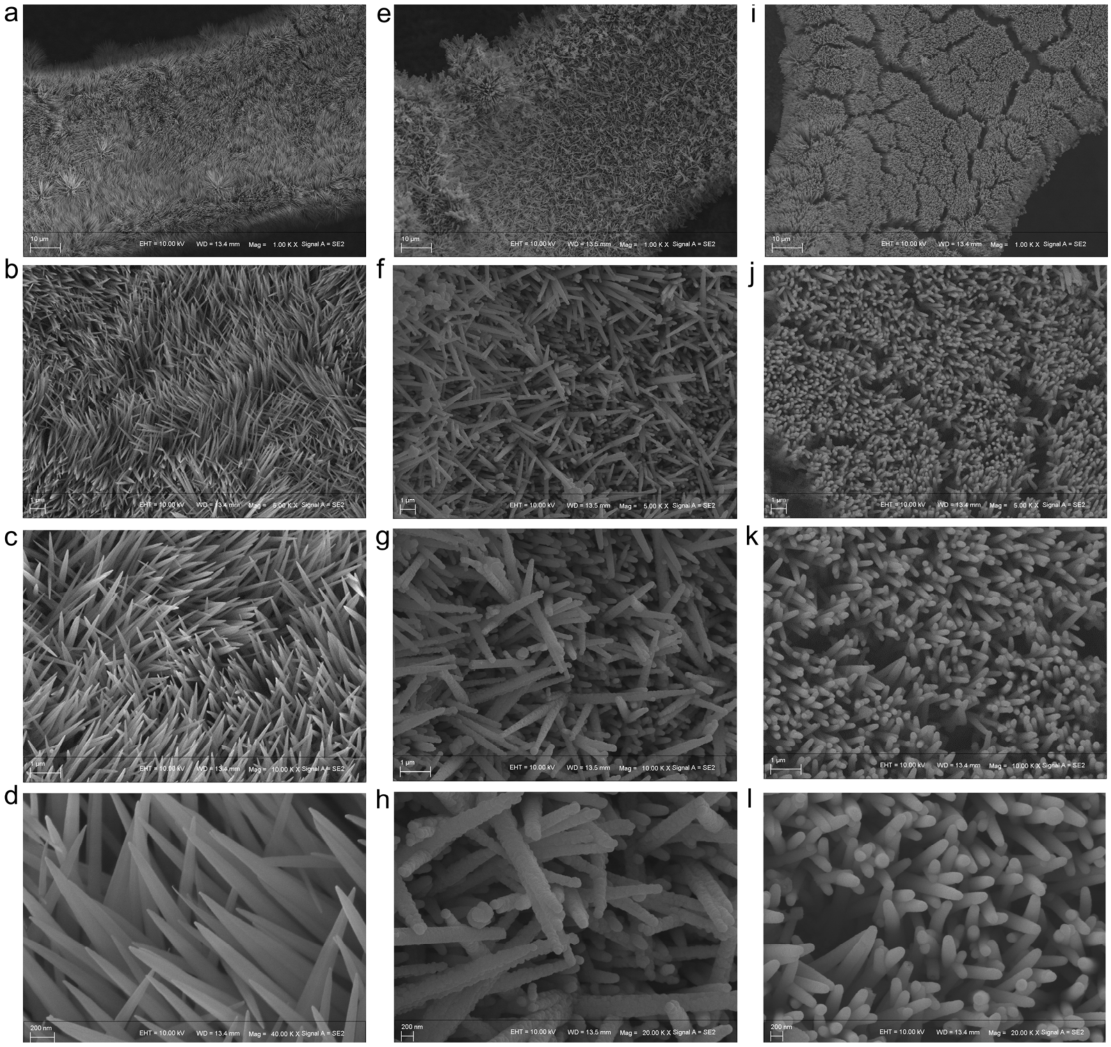

Fig. S3 SEM images of (a-d) Ni/Co-precursor/NF, (e-h) Mo-PDA@Ni/Co-precursor/NF, and (i-l) Mo_2N@NiCo/NF.

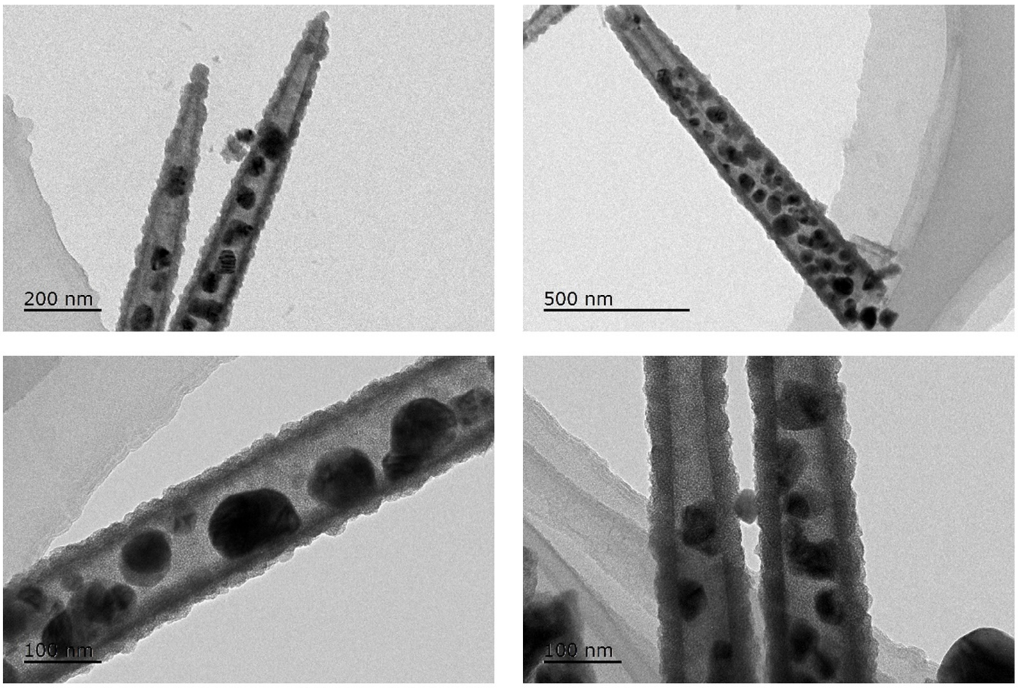

Fig. S4 TEM image of Mo_2N@NiCo/NF.

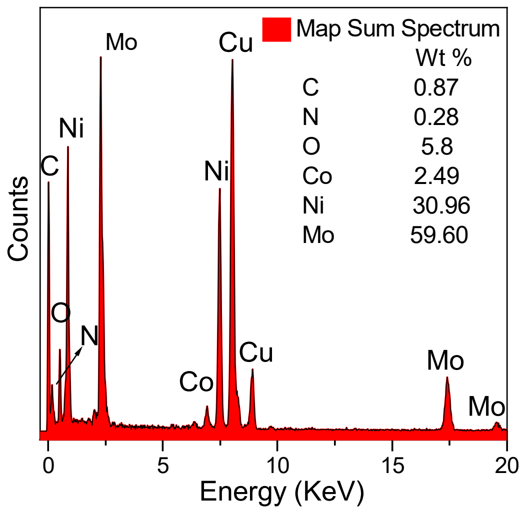

Fig. S5 EDX spectrum of Mo_2N@NiCo/NF.

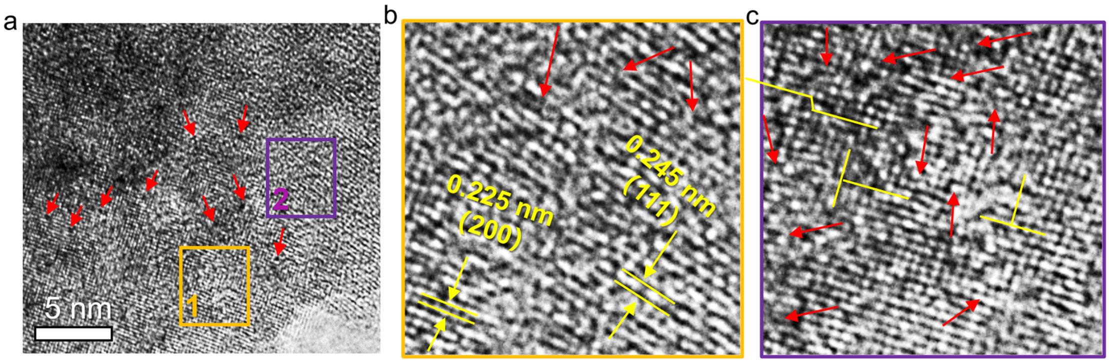

Fig. S6 High-resolution TEM images of Mo_2N@NiCo/NF.

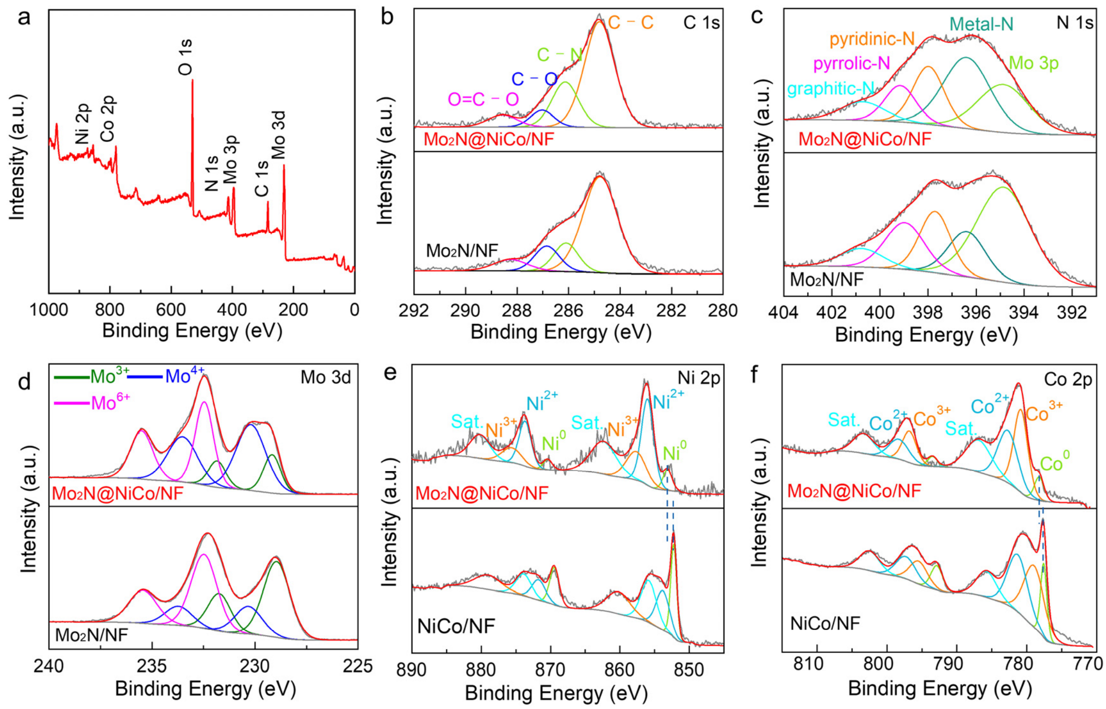

Fig. S7 Full-scan XPS spectrum (a) and high-resolution XPS spectra of (b) C 1s, (c) N 1s, (d) Mo 3d, (e) Ni 2p, and (f) Co 2p of Mo_2N@NiCo/NF, Mo_2N/NF, and NiCo/NF.

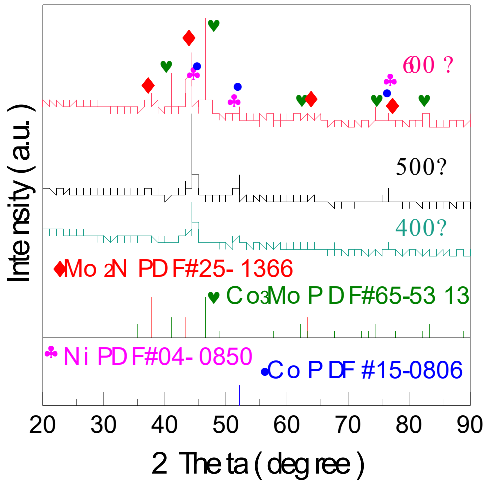

Fig. S8 XRD patterns of the annealing products of Mo-PDA@Ni/Co-precursor/NF at different temperatures (400, 500, and 600 °C).

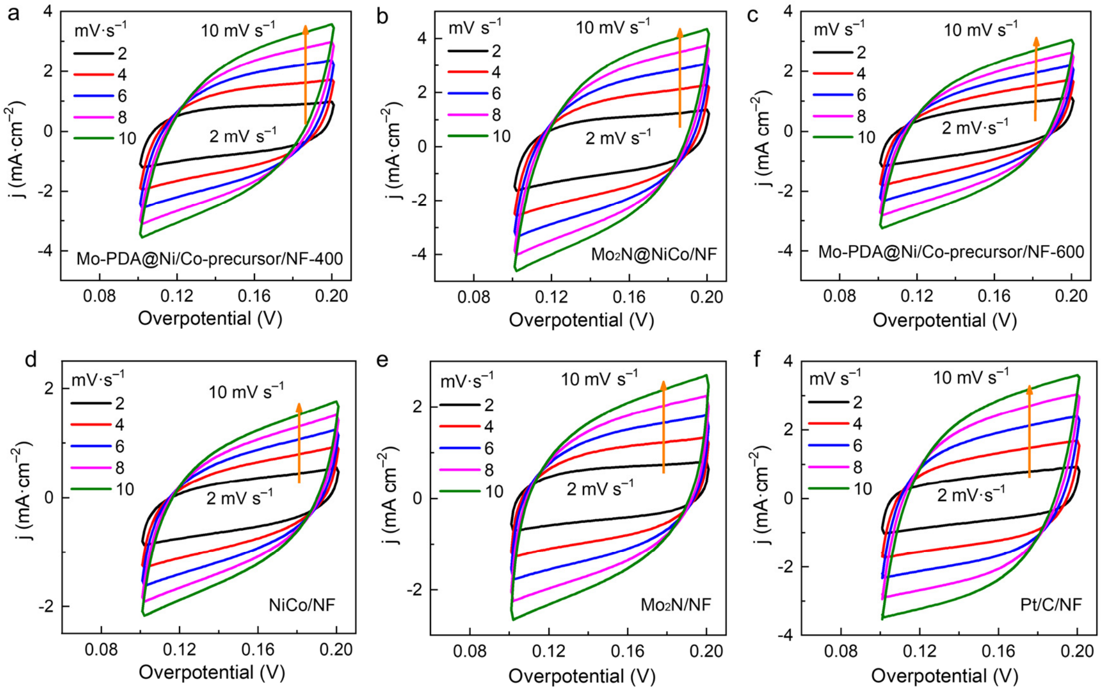

Fig. S9 CV curves of (a-f) all catalysts at different scan rates in the range of 2 to 10 mV·s^{-1} in 1 M KOH.

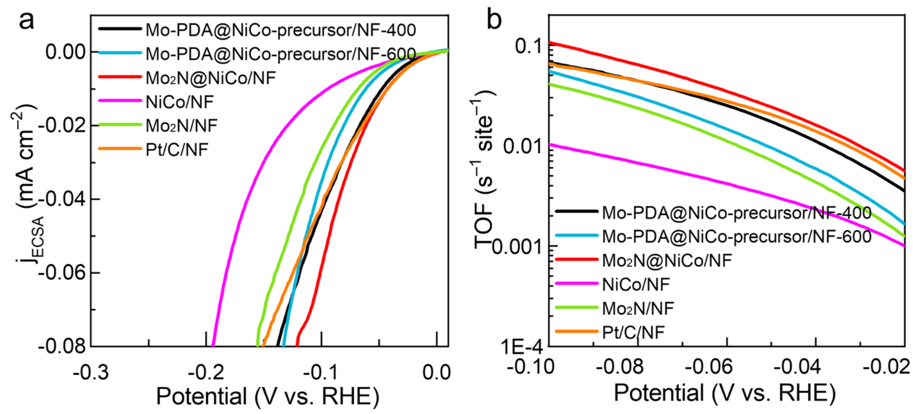

Fig. S10 (a) HER polarization curves normalized by ESCA and (b) TOF values of all samples.

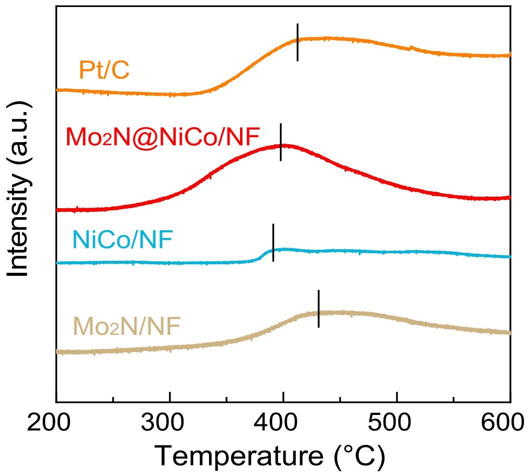

Fig. S11 H_2-TPD curves of as-prepared samples.

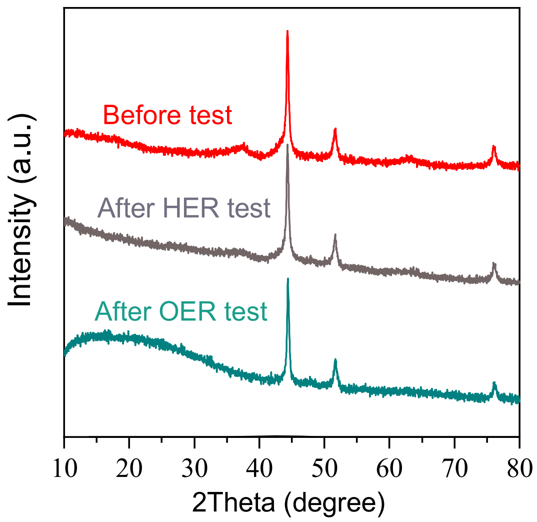

Fig. S12 XRD patterns of Mo_2N@NiCo/NF for HER and OER before and after long-term stability test.

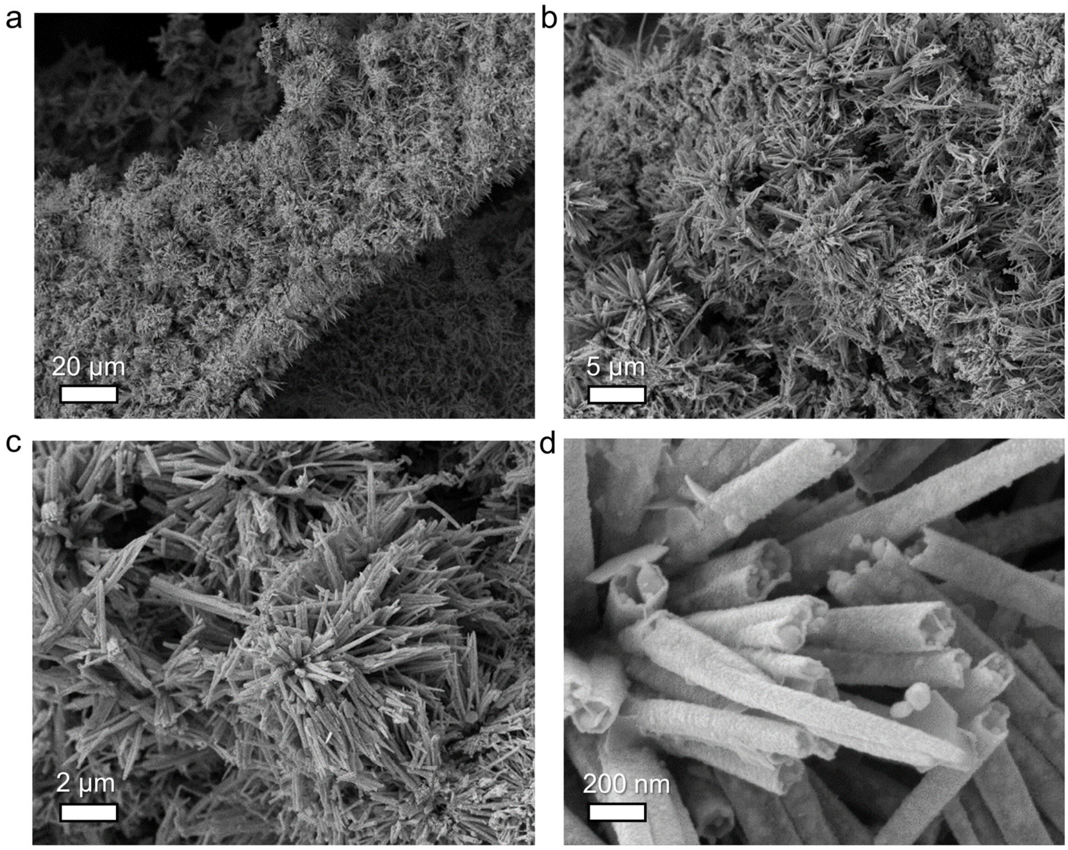

Fig. S13 SEM images of Mo_2N@NiCo/NF for HER after long-term stability test

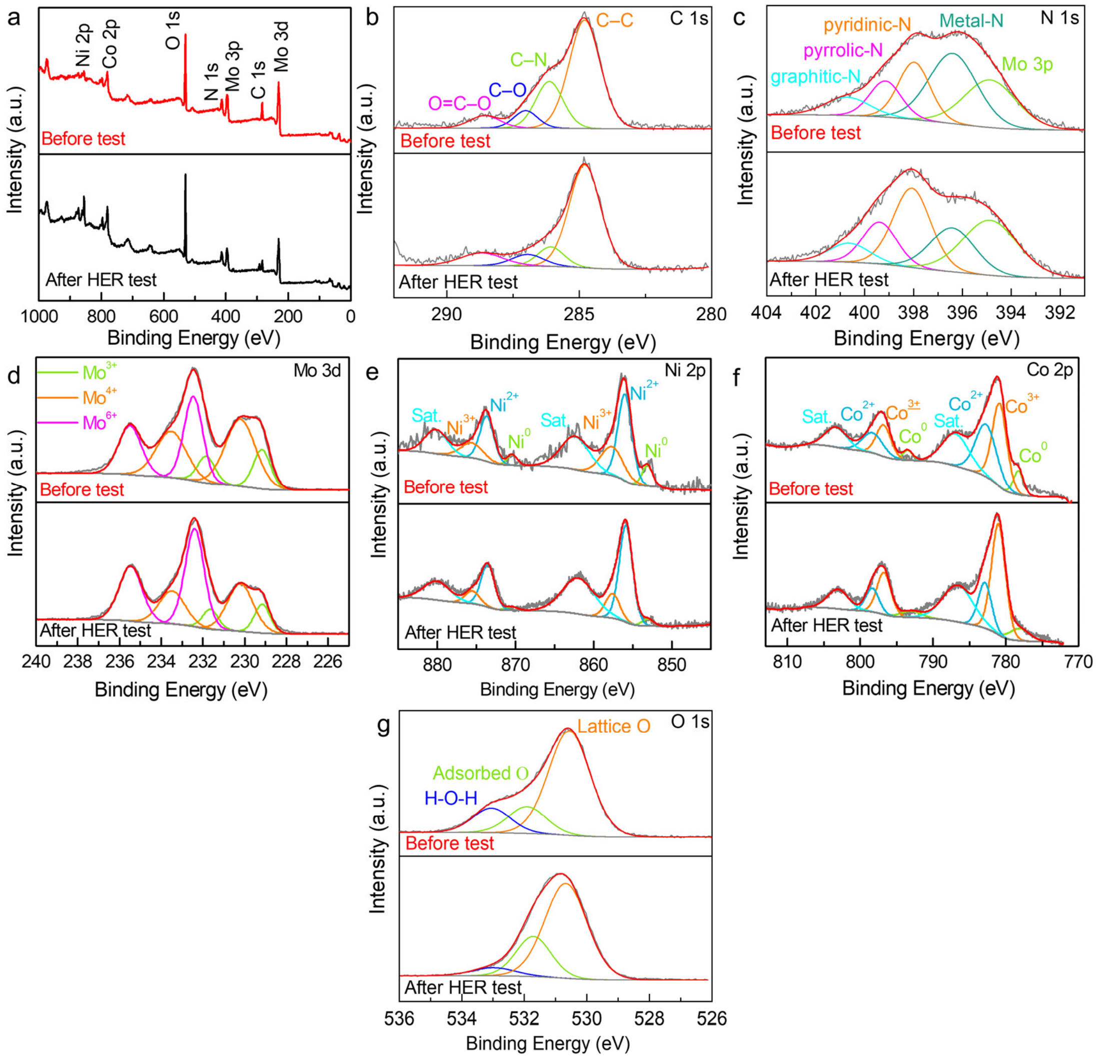

Fig. S14 Survey XPS spectra (a), and high-resolution XPS spectra of C 1s (b), N 1s (c), Mo 3d (d), Ni 2p (e), Co 2p (f), and O 1s (g) of Mo_2N@NiCo/NF for HER before and after stability testing.

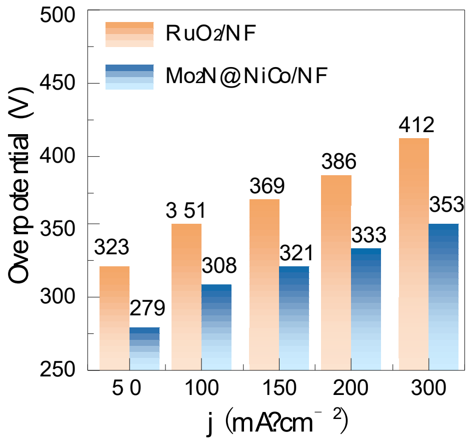

Fig. S15 Comparison of the overpotentials for OER performances of Mo_2N@NiCo/NF with RuO_2/NF

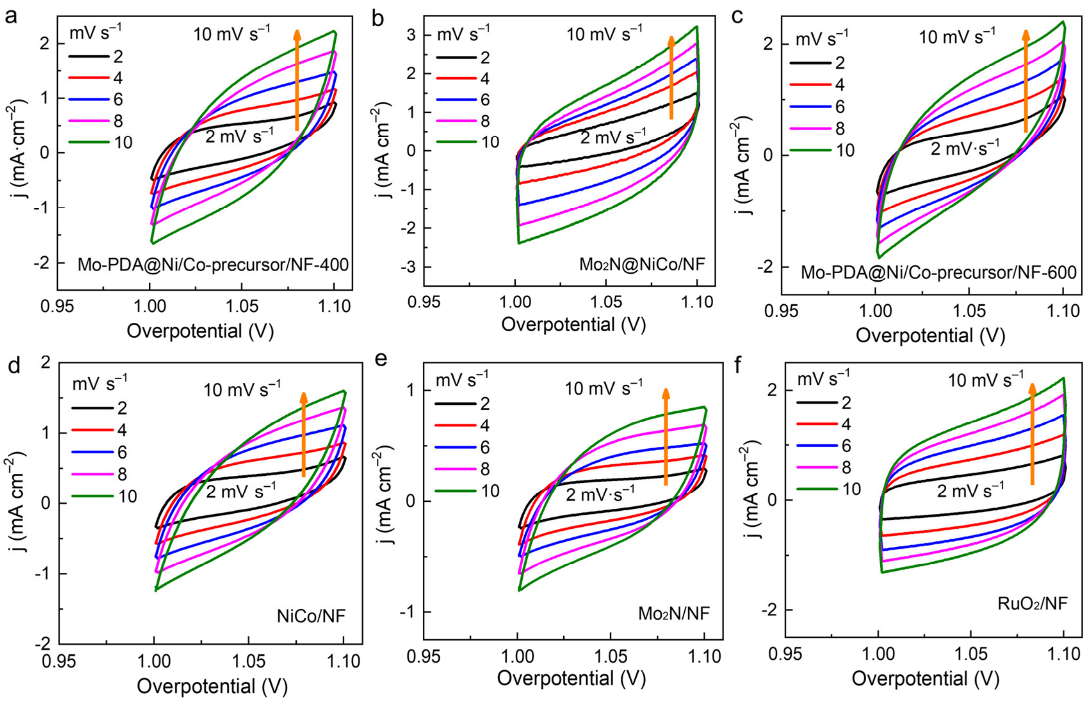

Fig. S16 CV curves at different scan rates in the range of 2 to 10 mV·s^{-1} for OER in 1 M KOH.

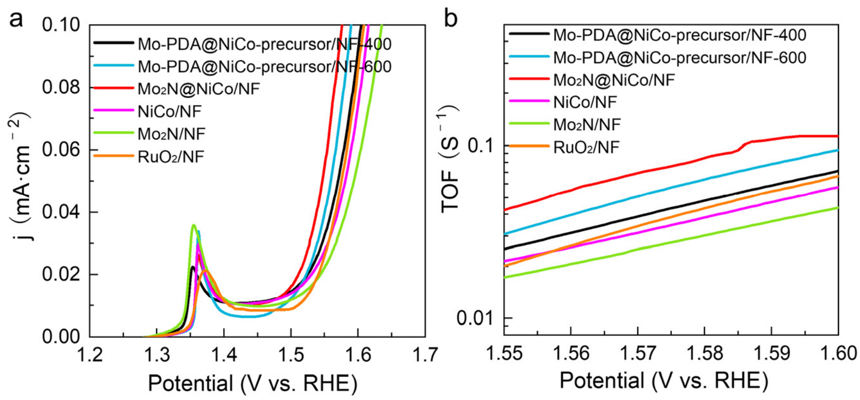

Fig. S17 (a) Polarization curves normalized by ESCA and (b) TOF values of all samples for OER.

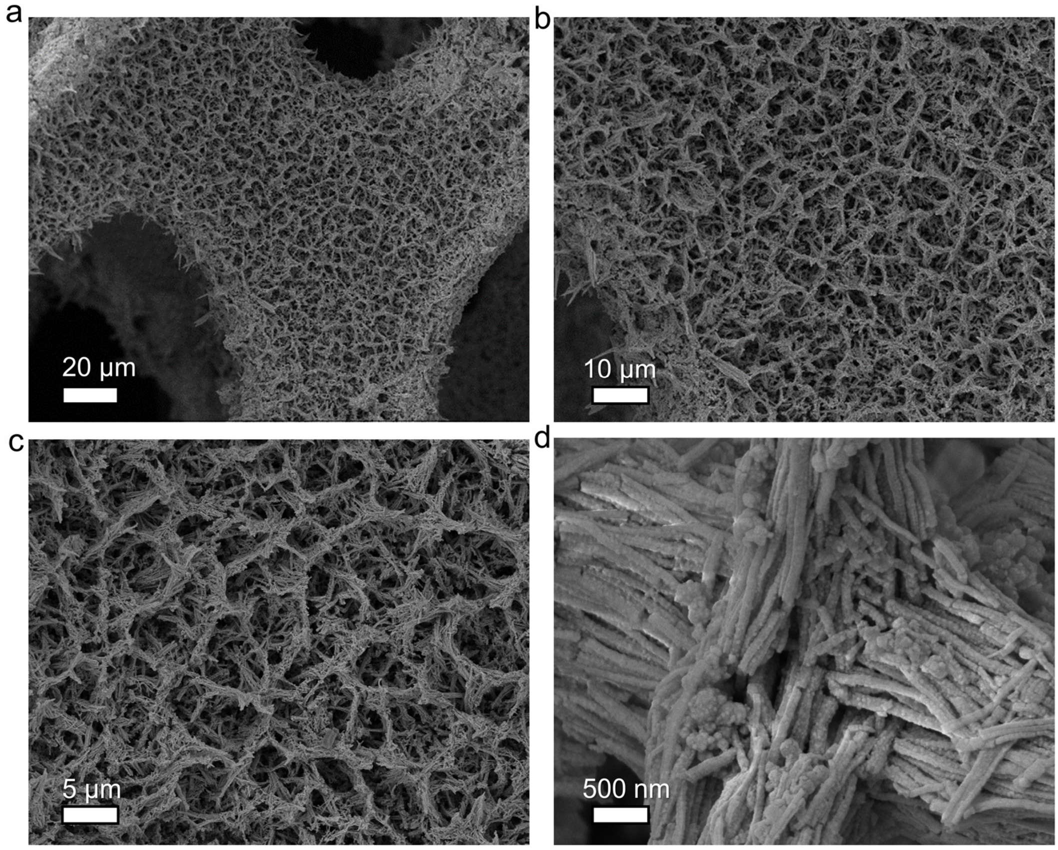

Fig. S18 SEM images of Mo_2N@NiCo/NF for OER after long-term stability test.

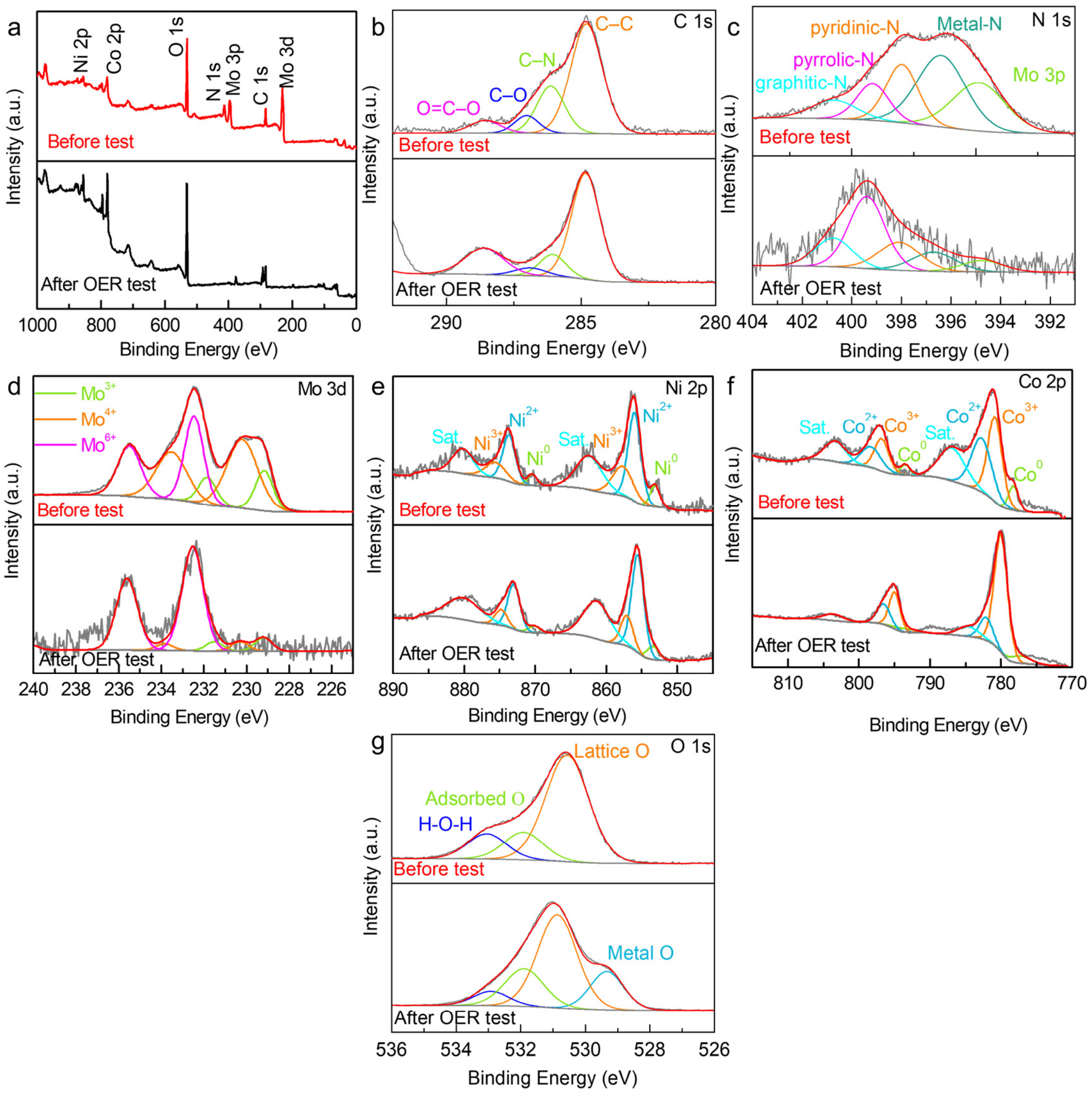

Fig. S19 Survey XPS spectra (a), and high-resolution XPS spectra of C 1s (b), N 1s (c), Mo 3d (d), Ni 2p (e), Co 2p (f), and O 1s of Mo_2N@NiCo/NF for OER before and after long-term stability test.

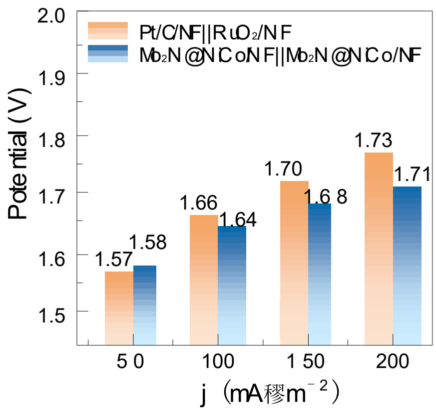

Fig. S20 Comparison of overpotentials for overall water splitting of Mo_2N@NiCo/NF || Mo_2N@NiCo/NF with Pt/C/NF || RuO_2/NF

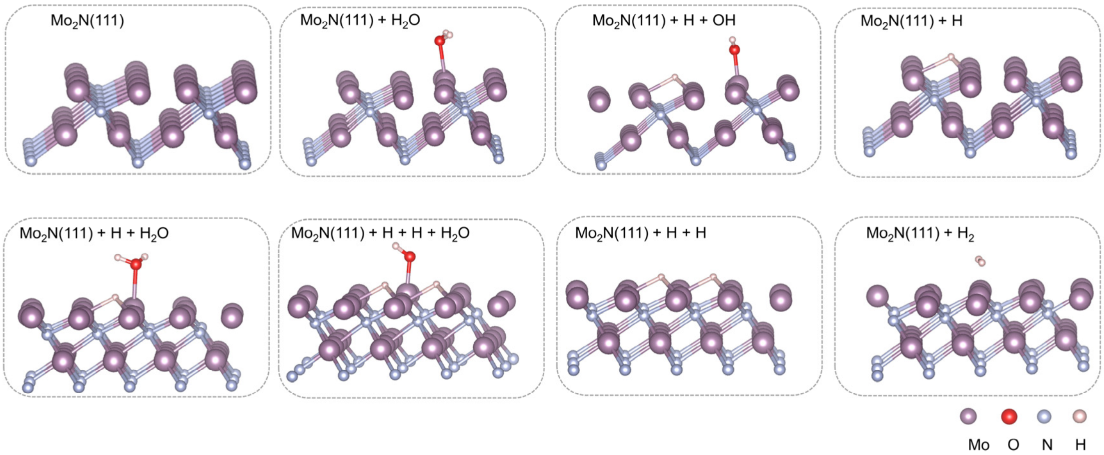

Fig. S21. The plots of different optimal simulated nanostructures of Mo_2N together with the water splitting processes on active sites.

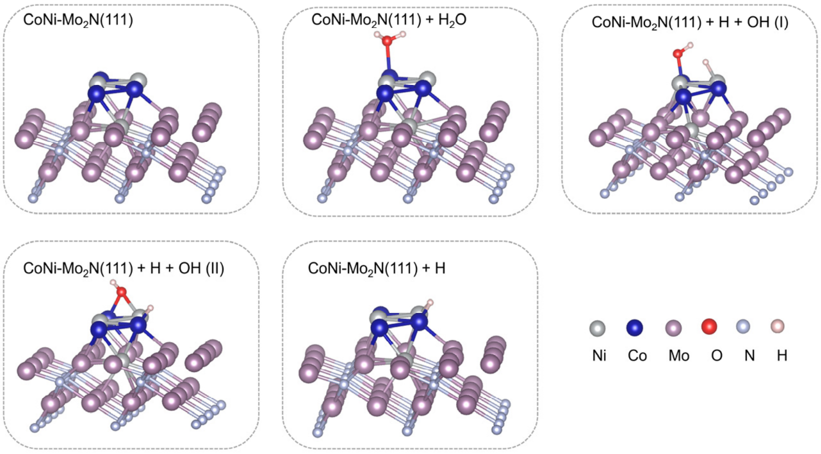

Fig. S22. The plots of different optimal simulated nanostructures of Mo_2N@CoNi together with the water splitting processes on reactive sites.

Table S1 Comparison of catalytic parameters of different HER electrocatalysts.

Electrocatalyst	η_{10} (mV)	η_{100} (mV)	Tafel slope (mV dec^{-1})	j_0 (mA·cm^{-2})	C_{dl} (mF·cm^{-2})	TOF$_{(20\ mV)}$ (s^{-1})	ECSA (cm^2)
Mo-PDA@Ni/Co-precursor/NF-400	30	89	34.2	1.67	185.6	3.6×10^{-3}	3093
Mo_2N@NiCo/NF	18	67	25.8	2.79	244.6	5.7×10^{-3}	4076
Mo-PDA@Ni/Co-precursor/NF-600	39	101	41.7	1.53	162.4	1.7×10^{-3}	2706
NiCo/NF	72	183	88.8	0.79	97.8	1.0×10^{-3}	1630
Mo_2N/NF	46	116	44.1	1.05	155.8	1.2×10^{-3}	2596
Pt/C/NF	21	87	30.2	2.16	184.8	4.8×10^{-3}	3080

Table S2 HER performances of the non-precious-metal electrocatalysts in alkaline media in recent reports.

Electrocatalyst	**η_{10} (mV)**	**η_{100} (mV)**	**Tafel slope (mV dec^{-1})**	**Refs**
Co/MoN	52	132	77.5	1
Ni-Mo	35	136	45.0	2
Ni-MoN/CF	24	61	35.5	3
$Ni_{2(1-x)}Mo_{2x}P$	72	162	46.4	4
N-NiMoS	68	135	86.0	5
G@$MoNi_4$-$NiMoO_4$/NF	55	190	38.0	6
Ni-Mo-N-500	55	125	61.4	7
Ni-Mo-N/NG	46	159	45.0	8
Co/CoMoN/NF	61	173	68.9	9
Co-MoN@NC	47	170	43.0	10
Co/NCNTs-NF	67	255	95.9	11
NiMoN/CC	109	168	95	12
Ni_2P/NF	80	175	76	13
Ni_3Fe@N-C	72	226	98	14
Mo_2N@NiCo/NF	18	67	25.8	This work

Table S3 OER parameters of various specimens

Electrocatalyst	η_{50} (mV)	η_{100} (mV)	η_{200} (mV)	Tafel slope (mV dec^{-1})	C_{dl} (mF·cm^{-2})	ECSA (cm^2)
Mo-PDA@Ni/Co-precursor/NF-400	309	341	376	106.5	114.7	1911
Mo_2N@NiCo/NF	279	308	333	86.6	154.5	2575
Mo-PDA@Ni/Co-precursor/NF-600	297	324	354	90.8	132.9	2215
NiCo/NF	322	357	393	114.8	79.1	1318
Mo_2N/NF	332	369	412	123.8	45.4	756
RuO_2/NF	323	351	386	91.5	106.3	1772

Table S4 OER performances of the non-precious-metal electrocatalysts in alkaline pure water in recent reports

Electrocatalyst	**η_{50} (mV)**	**η_{100} (mV)**	**Tafel 斜率 ($mV\ dec^{-1}$)**	**Refs.**
FeCoNi-ATNs/NF	340	412	52.7	15
Co@TiO_2/Ti-8h	382	465	142	16
K-ZIF-67-Ac-800	350	412	56.87	17
$NiCo_2O_4$ NT	346	383	89.8	18
$LaCo_2P_2$	440	460	57	19
N-Ni_3S_2	335	355	70	20
CoFe-NA2/NF	305	353	69.9	21
K-ZIF-67-Ac-800	350	411	56.87	17
NiCoFe-211	353	368	51.9	22
Co-Ni-P-2	393	410	67	23
CoFe-NA/NF	302	336	69.9	21
$MoNi_4$-MoO_2/CC	369	517	136	24
FeCoNi-ATNs/NF	340	370	52.7	15
Mo_2N@NiCo/NF	279	308	86.6	This work

Table S5 Comparison of the overall water splitting performances of various bifunctional electrocatalysts in alkaline pure water (1 M KOH).

Electrocatalyst	**η_{50} (V)**	**η_{100} (V)**	**Stable time (h)**	**Refs.**
3DP GC/NiFeP || 3DP GC/NiFeP	1.64	1.74	10	[25]
CoP-NC@NFP || CoP-NC@NFP	1.83	1.97	8	[26]
$Co_{0.43}Ni_{0.57}$@C || $Co_{0.43}Ni_{0.57}$@C	1.82	1.91	24	[27]
FeCoNi/CC || FeCoNi/CC	1.86	2.00	12	[15]
Co_7Fe_3-P/C || Co_7Fe_3-P/C	1.74	1.76	30	[28]
Ni-Mo-P || Ni-Mo-P	1.68	1.85	40	[29]
FeCo/Co_2P || FeCo/Co_2P	1.90	1.98	11	[30]
LiCoBPO || LiCoBPO	1.67	1.72	90	[31]
NiCoP@NC || NiCoP@NC	1.63	1.70	15	[32]
Ni-ZIF/NiB || Ni-ZIF/NiB	1.73	1.78	64	[33]
CoP/NCNHP || CoP/NCNHP	1.83	1.90	36	[34]
Co/NCNTs-NF || Co/NCNTs-NF	1.68	1.72	25	[11]
CoMoNx NSAs/NF || CoMoNx NSAs/NF	1.76	1.86	100	[35]
Mo-Ni_2P@NiFe/NF || Mo-	1.73	1.81	18	[36]

Ni_2P@NiFe/NF				
Mo_2N@NiCo/NF || Mo_2N@NiCo/NF	1.58	1.64	200	This work

Table S6 Comparison of the HER/OER and overall water splitting (OWS) performances of various bifunctional electrocatalysts in simulated seawater.

Electrocatalyst		η_{10} (V)	η_{50} (V)	η_{100} (V)	Refs.
CNFMPO	HER	73	200	290	37
	OER	282	360	420	
	OWS	1.56	1.78	2.1	
Er-MoO_2	HER	221	248	281	38
	OER	312	390	430	
	OWS	1.67	1.9	2.2	
C/CoP-FeP/FF	HER	100	162	190	39
	OER	-	286	310	
	OWS	-	1.7	1.75	
Mo-CoPx/NF	HER	150	220	310	40
	OER	250	355	420	
	OWS	-	1.8	1.97	
Ni/NCT	HER	200	320	284	41
	OER	-	-	-	
	OWS	-	-	-	
FMCO/NF	HER	120	248	395	42
	OER	302	328	350	
	OWS	1.58	1.73	1.98	
NiFe-P/NC	HER	-	-	-	43
	OER	-	320	360	
	OWS	-	1.77	1.93	
Mo_2N@NiCo/NF	HER	49	95	125	This work
	OER	-	238	317	

OWS	-	1.61	1.69

ECSA calculation:

The electrochemical surface areas (ECSA) of the samples were obtained based on the following equation:

$$ECSA = \frac{C_{dl}}{C_s}$$

where C_s is a standard value of 60 μF·cm^{-2} [37]

The ECSA in Mo_2N@NiCo/NF-400, Mo_2N@NiCo/NF-500, Mo_2N@NiCo/NF-600, NiCo/NF, Mo_2N/NF and Pt/C/NF were about 3093, 4076, 2706, 1630, 2596 and 3080 cm^2, respectively for HER. The ECSA in Mo_2N@NiCo/NF-400, Mo_2N@NiCo/NF-500, Mo_2N@NiCo/NF-600, NiCo/NF, Mo_2N/NF and RuO_2@NF were about and 1911, 2575, 2215, 1318, 756 and 1772 cm^2, respectively for OER.

Elucidation of turnover frequency (TOF)

The TOF is calculated by the following equation [5, 44]:

$$\mathrm{TOF} = \frac{The\ number\ of\ total\ hydrogen\ turnover\ per\ cm^2}{The\ number\ of\ surface\ active\ sites\ per\ cm^2}$$

$$= \frac{The\ number\ of\ total\ hydrogen\ turnover \times |j|}{active\ sites \times ECSA}$$

The number of total hydrogen turnovers is calculated from the current density using the following equation:

$$\left(\mathrm{j}\frac{mA}{cm^2}\right)\left(\frac{1\ C \cdot s^{-1}}{1000\ mA}\right)\left(\frac{1\ mol\ H_2}{96485.3\ C}\right)\left(\frac{1\ mol\ H_2}{2\ mol \cdot e^{-1}}\right)\left(\frac{6.02 \times 10^{23}\ molecules\ H_2}{1\ mol\ H_2}\right)$$

$$= 3.12 \times 10^{15} \frac{H_2/s}{cm^2} per \frac{mA}{cm^2}$$

Similarly, the number of total Oxygen turnovers is $1.56 \times 10^{15} \frac{O_2/s}{cm^2} per \frac{mA}{cm^2}$

Thus, The TOF values for the HER of Mo_2N@NiCo/NF-500 calculated to be:

$$\mathrm{TOF} = \frac{3.12 \times 10^{15} \frac{H_2/s}{cm^2} per \frac{mA}{cm^2} \times |j|}{2 \times 10^{15} atom \cdot per \cdot cm^2 \times ECSA}$$

$$= \frac{3.12 \times 10^{15} \frac{H_2/s}{cm^2} per \frac{mA}{cm^2} \times |j| \frac{mA}{cm^2}}{2 \times 10^{15} atom \cdot per \cdot cm^2 \times 4076 \;\; cm^2}$$

Similarly, the TOF of Mo_2N@NiCo/NF-400, Mo_2N@NiCo/NF-600, NiCo/NF and Mo_2N/NF can be calculated:

Mo_2N@NiCo/NF-400:

$$\mathrm{TOF} = \frac{3.12 \times 10^{15} \frac{H_2/s}{cm^2} per \frac{mA}{cm^2} \times |j| \frac{mA}{cm^2}}{2 \times 10^{15} atom \cdot per \cdot cm^2 \times 3093 \;\; cm^2}$$

Mo_2N@NiCo/NF-600:

$$\mathrm{TOF} = \frac{3.12 \times 10^{15} \frac{H_2/s}{cm^2} per \frac{mA}{cm^2} \times |j| \frac{mA}{cm^2}}{2 \times 10^{15} atom \cdot per \cdot cm^2 \times 2706 \;\; cm^2}$$

NiCo/NF:

$$\mathrm{TOF} = \frac{3.12 \times 10^{15} \frac{H_2/s}{cm^2} per \frac{mA}{cm^2} \times |j| \frac{mA}{cm^2}}{2 \times 10^{15} atom \cdot per \cdot cm^2 \times 1630 \;\; cm^2}$$

Mo_2N/NF:

$$\mathrm{TOF} = \frac{3.12 \times 10^{15} \frac{H_2/s}{cm^2} per \frac{mA}{cm^2} \times |j| \frac{mA}{cm^2}}{2 \times 10^{15} atom \cdot per \cdot cm^2 \times 2596 \;\; cm^2}$$

Pt/C/NF:

$$\mathrm{TOF} = \frac{3.12 \times 10^{15} \frac{H_2/s}{cm^2} per \frac{mA}{cm^2} \times |j| \frac{mA}{cm^2}}{2 \times 10^{15} atom \cdot per \cdot cm^2 \times 3080 \;\; cm^2}$$

References

1. Sun, J.W. *et al.* Co/MoN hetero-interface nanoflake array with enhanced water dissociation capability achieves the Pt-like hydrogen evolution catalytic performance. *Appl. Catal. B-Environ.* **286**, 119882 (2021).
2. Zhang, Q. *et al.* Superaerophobic Ultrathin Ni-Mo Alloy Nanosheet Array from In Situ Topotactic Reduction for Hydrogen Evolution Reaction. *Small* **13**, 1701648 (2017).
3. Wu, L.B. *et al.* Efficient Alkaline Water/Seawater Hydrogen Evolution by a Nanorod-Nanoparticle-Structured Ni-MoN Catalyst with Fast Water-Dissociation Kinetics. *Adv. Mater.* **34**, 2201774 (2022).
4. Yu, L. *et al.* Ternary $Ni_{2(1-x)}Mo_{2x}P$ nanowire arrays toward efficient and stable hydrogen evolution electrocatalysis under large-current-density. *Nano Energy* **53**, 492-500 (2018).
5. Huang, C.Q. *et al.* N-doped Ni-Mo based sulfides for high-efficiency and stable hydrogen evolution reaction. *Appl. Catal. B-Environ.* **276**, 119137 (2020).
6. An, L.H. *et al.* Graphene layer encapsulated $MoNi_4$-$NiMoO_4$ for electrocatalytic water splitting. *Appl. Surf. Sci.* **504**, 144390 (2020).
7. Wang, Z.N. *et al.* Integrating Ni nanoparticles into MoN nanosheets form Schottky heterojunctions to boost its electrochemical performance for water electrolysis. *J. Alloy. Compd.* **867**, 158983 (2021).
8. Xue, S. *et al.* Heterostructured Ni-Mo-N nanoparticles decorated on reduced graphene oxide as efficient and robust electrocatalyst for hydrogen evolution reaction. *Carbon* **165**, 122-128 (2020).
9. Ma, H.B., Chen, Z.W., Wang, Z.L., Singh, C.V. & Jiang, Q. Interface Engineering of Co/CoMoN/NF Heterostructures for High-Performance Electrochemical Overall Water Splitting. *Adv. Sci.* **9**, 2105313 (2022).
10. Lang, X.W. *et al.* A Co-Mo_2N composite on a nitrogen-doped carbon matrix with hydrogen evolution activity comparable to that of Pt/C in alkaline media. *J. Mater. Chem. A* **7**, 20579-20583 (2019).
11. Liu, J. *et al.* Metal-Organic-Framework-Derived Cobalt nanoparticles encapsulated in Nitrogen-Doped carbon nanotubes on Ni foam integrated Electrode: Highly electroactive and durable catalysts for overall water splitting. *J. Colloid Interface Sci.* **606**, 38-46 (2022).
12. Zhang, Y. *et al.* 3D porous hierarchical nickel-molybdenum nitrides synthesized by RF plasma as highly active and stable hydrogen-evolution-reaction electrocatalysts. *Adv. Energy Mater.* **6**, 1600221 (2016).
13. Yu, X. *et al.* "Superaerophobic" nickel phosphide nanoarray catalyst for efficient hydrogen evolution at ultrahigh current densities. *J. Am. Chem. Soc.* **141**, 7537-7543 (2019).

14. Li, T.F. *et al.* Encapsulation of Ni_3Fe Nanoparticles in N-Doped Carbon Nanotube-Grafted Carbon Nanofibers as High-Efficiency Hydrogen Evolution Electrocatalysts. *Adv. Funct. Mater.* **28**, 1805828 (2018).
15. Zhang, Q.R., Bedford, N.M., Pan, J., Lu, X.Y. & Amal, R. A Fully Reversible Water Electrolyzer Cell Made Up from FeCoNi (Oxy)hydroxide Atomic Layers. *Adv. Energy Mater.* **9**, 1901312 (2019).
16. Yang, C.H. *et al.* Cobalt nanorods decorated titanium oxide arrays as efficient and stable electrocatalyst for oxygen evolution reaction. *Electrochim. Acta* **396**, 139213 (2021).
17. Chang, J.L. *et al.* Cobalt nanoparticles embedded nitrogen doped carbon, preparation from alkali deprotonation assisted ZIF-67 and its electrocatalytic performance in oxygen evolution reaction. *Int. J. Hydrogen Energy* **45**, 12787-12797 (2020).
18. Zhang, L., Li, Y.y., Peng, J.h. & Peng, K. Bifunctional $NiCo_2O_4$ porous nanotubes electrocatalyst for overall water-splitting. *Electrochim. Acta* **318**, 762-769 (2019).
19. Mann, D.K. *et al.* Polar Layered Intermetallic $LaCo_2P_2$ as a Water Oxidation Electrocatalyst. *ACS Appl. Mater. Inter.* **14**, 14120-14128 (2022).
20. Chen, P.Z. *et al.* 3D Nitrogen-Anion-Decorated Nickel Sulfides for Highly Efficient Overall Water Splitting. *Adv. Mater.* **29**, 1701584 (2017).
21. Chen, M.P. *et al.* Remarkable synergistic effect in cobalt-iron nitride/alloy nanosheets for robust electrochemical water splitting. *J. Energy Chem.* **65**, 405-414 (2022).
22. Wang, Z.J., Jin, M.X., Zhang, L., Wang, A.J. & Feng, J.J. Amorphous 3D pomegranate-like NiCoFe nanoassemblies derived by bi-component cyanogel reduction for outstanding oxygen evolution reaction. *J. Energy Chem.* **53**, 260-267 (2021).
23. Pei, Y. *et al.* Controlled Electrodeposition Synthesis of Co-Ni-P Film as a Flexible and Inexpensive Electrode for Efficient Overall Water Splitting. *ACS Appl. Mater. Inter.* **9**, 31887-31896 (2017).
24. Tian, G. *et al.* Preparation of highly active $MoNi_4$ alloys in 3D porous nanostructures and their application as bifunctional electrocatalysts for overall water splitting. *Catal. Commun.* **159**, 106350 (2021).
25. Peng, M.W. *et al.* 3D Printed Mechanically Robust Graphene/CNT Electrodes for Highly Efficient Overall Water Splitting. *Adv. Mater.* **32**, 1908201 (2020).
26. Vijayakuma, E. *et al.* MOF-derived CoP-nitrogen-doped carbon@NiFeP nanoflakes as an efficient and durable electrocatalyst with multiple catalytically active sites for OER, HER, ORR and rechargeable zinc-air batteries. *Chem. Eng. J.* **428**, 131115 (2022).
27. Wang, X.Y. *et al.* Coordination confinement pyrolysis to hollow sea urchin shaped composite with embedded ultrasmall Co/Ni alloy for overall water splitting. *Int. J. Hydrogen Energy* **47**, 3699-3708 (2022).

28. Peng, Z.G. *et al.* Gap channel carbon layer coated bimetallic CoFe phosphate as a bifunctional electrocatalyst for overall water splitting. *J. Power Sources* **538**, 231571 (2022).
29. Zhang, B. *et al.* Phosphorus doped nickel-molybdenum aerogel for efficient overall water splitting. *Appl. Catal. B-Environ.* **298**, 120494 (2021).
30. Shi, Q. *et al.* High-Performance Trifunctional Electrocatalysts Based on FeCo/Co_2P Hybrid Nanoparticles for Zinc-Air Battery and Self-Powered Overall Water Splitting. *Adv. Energy Mater.* **10**, 1903854 (2020).
31. Menezes, P.W. *et al.* Helical cobalt borophosphates to master durable overall water-splitting. *Energy Environ. Sci.* **12**, 988-999 (2019).
32. Cao, B. *et al.* Efficient and Durable 3D Self-Supported Nitrogen-Doped Carbon-Coupled Nickel/Cobalt Phosphide Electrodes: Stoichiometric Ratio Regulated Phase- and Morphology- Dependent Overall Water Splitting Performance. *Adv. Funct. Mater.* **29**, 1906316 (2019).
33. Xu, H.B. *et al.* Boronization-induced ultrathin 2D nanosheets with abundant crystalline-amorphous phase boundary supported on nickel foam toward efficient water splitting. *Adv. Energy Mater.* **10**, 1902714 (2020).
34. Pan, Y. *et al.* Core-Shell ZIF-8@ZIF-67-Derived CoP Nanoparticle-Embedded N-Doped Carbon Nanotube Hollow Polyhedron for Efficient Overall Water Splitting. *J. Am. Chem. Soc.* **140**, 2610-2618 (2018).
35. Lu, Y.K. *et al.* Bimetallic Co-Mo nitride nanosheet arrays as high-performance bifunctional electrocatalysts for overall water splitting. *Chem. Eng. J.* **411**, 128433 (2021).
36. Yang, Z. *et al.* In situ growth of 3D walnut-like nano-architecture Mo-Ni_2P@NiFe LDH/NF arrays for synergistically enhanced overall water splitting. *J. Energy Chem.* **49**, 189-197 (2020).
37. Zhang, H.-M. *et al.* Amorphous high-entropy phosphoxides for efficient overall alkaline water/seawater splitting. *Journal of Materials Science & Technology* **173**, 1-10 (2024).
38. Yang, T. *et al.* Electronic structure modulation of MoO_2 via Er-doping for efficient overall water/seawater splitting and Mg/seawater batteries. *Applied Surface Science* **615**, 156360 (2023).
39. Li, J., Hu, Y., Huang, X., Zhu, Y. & Wang, D. Bimetallic Phosphide Heterostructure Coupled with Ultrathin Carbon Layer Boosting Overall Alkaline Water and Seawater Splitting. *Small* **19**, 2206533 (2023).
40. Yu, Y. *et al.* Mo-decorated cobalt phosphide nanoarrays as bifunctional electrocatalysts for efficient overall water/seawater splitting. *Materials Today Nano* **18**, 100216 (2022).
41. Ghosh, A., T K, S.F., Ganguly, D. & Sundara, R. CoFePBA Nanosheets on Carbon Nanotubes Coupled with Nickel-Encapsulated Carbon Tubules for Efficient and Highly Stable Overall Seawater Electrolysis. *ACS Applied Energy Materials* **6**, 6080-6090 (2023).

42. Liu, W. *et al.* Ferrum-molybdenum dual incorporated cobalt oxides as efficient bifunctional anti-corrosion electrocatalyst for seawater splitting. *Applied Catalysis B: Environmental* **328**, 122488 (2023).
43. Chen, Z. *et al.* Hierarchical porous NiFe-P@NC as an efficient electrocatalyst for alkaline hydrogen production and seawater electrolysis at high current density. *Inorg. Chem. Front.* **10**, 1493-1500 (2023).
44. Wei, H.F. *et al.* Incorporating ultra-small N-doped Mo_2C nanoparticles onto 3D N-doped flower-like carbon nanospheres for robust electrocatalytic hydrogen evolution. *Nano Energy* **86**, 106047 (2021).